J. Astrophys. Astr. (2020) 41:6
https://doi.org/10.1007/s12036-020-9621-2

Vilnius photometry and Gaia astrometry of Melotte 105

TIMOTHY BANKS[1,*], TALAR YONTAN[2], SELÇUK BILIR[3] and REMZIYE CANBAY[2]

[1]Nielsen, Data Science, 200 W Jackson Blvd #17, Chicago, IL 60606, USA.
[2]Programme of Astronomy and Space Sciences, Institute of Graduate Studies in Science, Istanbul University, 34116 Beyazıt, Istanbul, Turkey.
[3]Department of Astronomy and Space Sciences, Faculty of Science, Istanbul University, 34119 University, Istanbul, Turkey.
*Corresponding author. E-mail: tim.banks@nielsen.com

MS received 25 September 2019; accepted 17 December 2019

Abstract. Archival Vilnius CCD photometric observations are presented for the heavily reddened star cluster Melotte 105, resulting in colour-magnitude diagrams and spectral class estimates. There is considerable lack of agreement between studies for reddening, age and distance for this cluster explaining why the archival data are being made available by this paper. The derived reddening $E(B-V) = 0.34 \pm 0.04$ mag and the distance $V - M_V = 12.9 \pm 0.3$ mag are directly from the Vilnius photometry. The *Gaia* Data Release 2 (DR2) and Vilnius photometric data of the cluster were used to estimate the structural parameters of the cluster, probability of stellar membership in the cluster, the distance modulus and the cluster age. Lack of Y band observations prevented determination of metal abundance. The values of the colour excess and distance module are determined by two different methods (i.e., Q and Zero Age Main Sequence or ZAMS methods). A distance modulus of 12.85 ± 0.07 mag was derived by ZAMS fitting, in good agreement with the above estimate. ZAMS fitting indicates a reddening of 0.403 ± 0.02 mag, within two sigma of the estimate above. The cluster's metallicity and age are estimated to be 0.24 dex and 240 ± 25 Myr, respectively. The derived mass function is in good agreement with the Salpeter slope. The cluster space velocity components (U, V, W) were determined as (-3.90 ± 3.34, -13.76 ± 5.69, $+3.45 \pm 0.41$) km/s. Perigalactic and apogalactic distances were obtained as $R_p = 6.85$ and $R_a = 7.44$ kpc respectively. The maximum vertical distance from the Galactic plane was calculated as $Z_{\max} = 84$ pc and the eccentricity of the orbit was determined as $e = 0.042$.

Keywords. Galaxy: open cluster and associations—individual: Melotte 105—photometry: Vilnius photometry.

1. Introduction

The seven filter intermediate band Vilnius system (see Straižys 1992a; Forbes 1996) makes possible the purely photometric determination of the spectral classes, absolute magnitudes and metallicities of stars while also correcting for interstellar reddening. This is facilitated by the careful thought given to the positioning and widths of the filters relative to the spectral features of all luminosity classes. For example, the U filter measures the ultraviolet intensity below the Balmer jump, while the P filter is placed on the jump itself, allowing luminosity determinations for early type stars. The X filter measures a wavelength range longer than the Balmer jump, between the H_δ and H_ϵ lines. This filter measures the continuum intensity after the Balmer jump for early-type stars, and the metallic-line blanketing for late-type stars. Y is centred around 466 nm, excluding the interstellar band at 433 nm and the H_γ line. The Z, V and S filters coincide with features in late-type stars (see Figure 1 of Dodd *et al.* 1993). Z is near the bottom of an absorption feature in late-type stars. The absorption intensity of the Mg II triplet lines and the Mg H band is measured. V measures the continuum at nearly the mean wavelength of the Johnson V filter. In conjunction with the Y filter, a direct conversion may be made to the Johnson BV system (Forbes 1996). S is centred on the H_α line at 656 nm. It is used to separate the B emission (Be) stars from normal B stars. The filter measures the absorption or emission intensity of the H_α

Published online: 04 March 2020

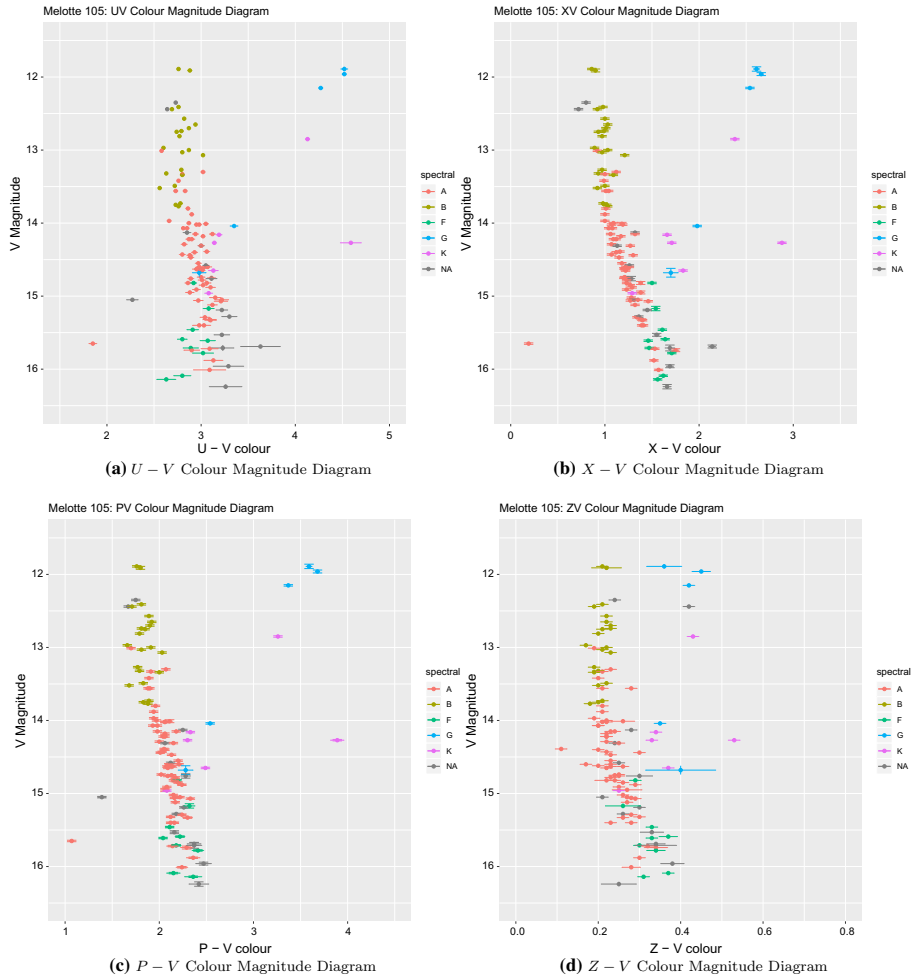

(a) $U-V$ Colour Magnitude Diagram **(b)** $X-V$ Colour Magnitude Diagram

(c) $P-V$ Colour Magnitude Diagram **(d)** $Z-V$ Colour Magnitude Diagram

Figure 1. Colour magnitude diagrams for Melotte 105 **(a)–(d)**, plotting the 'standard' colour indices for the Vilnius system. Data points are coloured according to the derived spectral class. 'NA' stands for 'not available', indicating those stars where the spectral class could not be derived.

line in early-type stars, or the pseudo-continuum (due to metallic lines) in late-type stars. Unlike the other filters which were, at the time of data collection for this paper, Soviet-made coloured glasses cemented with Canadian Balsam, the S filter is an interference filter. Peculiar stars, such as metal-deficient giants and blue horizontal branch stars, can be recognised using the two- and three-dimensional classification schemes of the system (Straižys 1992a; Straiž̌y 1992b), making the filter set well suited for the study of star clusters. Further, details of the rationale in the design of the filter set may be found in Straižys and Sviderskienė (1972).

The Vilnius colour indices $U-P$, $P-X$, $X-Y$, $Y-Z$, $Z-Y$, and $V-S$ are set to zero for unreddened O-type stars. Colours for all normal stars are therefore positive. In light of these capabilities, the idea of extending the system to the southern hemisphere was first considered in 1985 at the Royal Observatory Edinburgh, given that none of the already established standard regions (e.g. Zdanavičus *et al.* 1969; Černies *et al.* 1989; Černies and Zdanavičus 1992) extended south of the celestial equator. This programme commenced in 1988 using the 61-cm telescopes at Mount John University Observatory (MJUO), with the initial goal of establishing standards near the South Celestial Pole and also bright ($V < 7$ mag) stars generally distributed south of -20 degrees. Many southern Vilnius standard stars have been established in NGC 4755. Further details on the programme may be found in Forbes (1993) and Dodd *et al.* (1993) (Figure 1).

2. Melotte 105

Melotte 105 is an open cluster that has not attracted much attention. It is a compact cluster located in

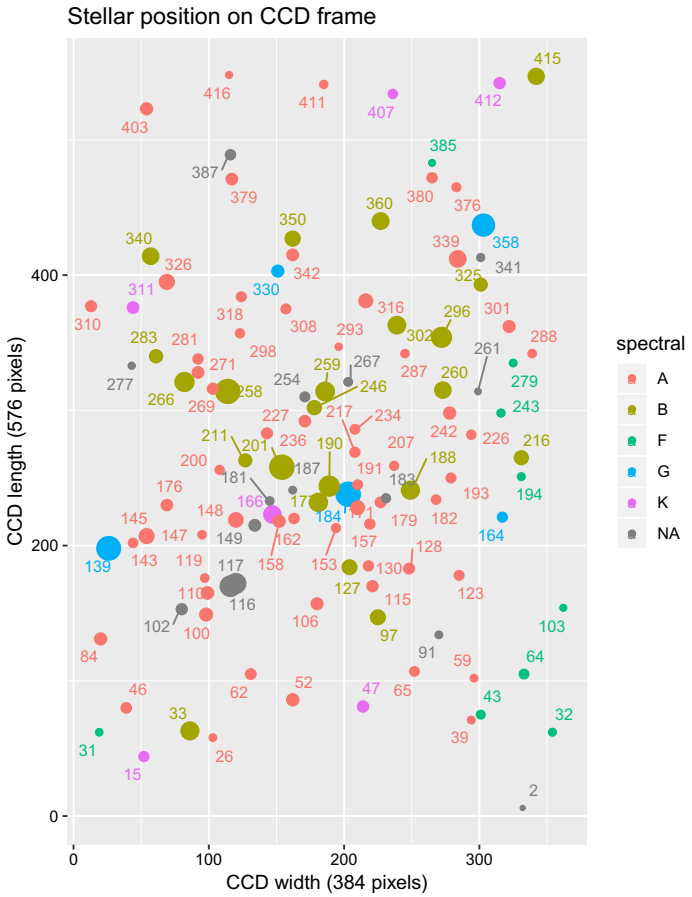

Figure 2. Positions and identifications of stars in Melotte 105: the radius of a point indicating the position of a star is proportional to the derived V magnitude of that star. The $UPXZVS$ magnitude, x and y positions, and identification numbers of the stars plotted in this figure are given in Table 2. A CCD pixel corresponds to 0.6 arcseconds at the $f/7.9$ Cassegrain focus of the Mclellan telescope.

the Galactic plane in the direction of Carina. In the literature, only a few studies have produced colour-magnitude diagrams for the cluster. The first was based on the *UBV* photoelectric and photographic photometry of Sher (1965), who estimated the cluster age via isochrone fits as $\sim 10^8$ years. As part of a search for small photometric fluctuations in giant and supergiant stars, Frandsen *et al.* (1989) produced a Johnson *BV* CMD based on CCD observations, which extended to $V \sim 19$ mag. The paper adopted the distance modulus $(V - M_V) = 12.7$ mag and reddening $E(B-V) = 0.38$ mag of Sher (1965). Kjeldsen and Frandsen (1991) re-observed the cluster and derived independent values for these parameters, $E(B-V)$ was estimated to be 0.52 ± 0.03 mag and $(V - M_V)$ as 13.35 ± 0.20 mag. The authors considered that the difference was due to the improved detector used, as well as the use of DAOphot (Stetson 1987) in this rather crowded field. However, Kjeldsen and Frandsen (1991) commented that the response of the CCD combined with the U and B filters used by their study differs substantially from the standard responses and that there were severe problems transforming their data across the standard system (Figure 2).

The cluster was the target of uvby CCD photometry by Balona and Laney (1995). Santos (1993) and Ahumada *et al.* (2000) performed integrated spectroscopic investigations (deriving $E(B-V) \sim 0.3$ mag). The reddening, distance and age values derived from all these studies vary substantially — by around 50%, 20% and 80% respectively. Piatti and Claria (2001) collected *BVI* CCD observations of the cluster, deriving $E(B-V) = 0.42 \pm 0.03$ mag, and a $(V - M_V)$ of 11.75 mag. Again, this is closer to Sher (1965) than to Kjeldsen and Frandsen (1991). This should be compared with a $E(B-V)$ of 0.46 mag derived from Balona and Laney (1995), Piatti and Claria (2001) and Sagar *et al.*'s (2001) value of 0.52 (no error given) based on *UBVRI* CCD photometry, which both lean towards the values of Kjeldsen and Frandsen (1991). It is

Table 1. Transformation co-efficients where m_1, m_2 and m_3 are as given in Equation (1). 'Std RMS' gives the expected RMS, given the formal uncertainties listed by Forbes (1996) for the standard stars, while 'RMS' is the root mean square error from the fits themselves. The column '#' indicates the number of standard star observations made per filter. 15 individual standards were observed, with a $(Y - V)$ colour range of 0.31 to 1.71. The air mass range was 1.0 to 1.8.

Filter	m_1	m_2	m_3	RMS	Std RMS	#
U	17.531 ± 0.030	-0.008 ± 0.007	0.654 ± 0.019	0.031	0.027	40
P	17.260 ± 0.031	$+0.091 \pm 0.006$	0.555 ± 0.019	0.032	0.023	47
X	17.488 ± 0.028	$+0.015 \pm 0.010$	0.365 ± 0.017	0.030	0.018	50
Z	17.622 ± 0.025	$+0.019 \pm 0.004$	0.136 ± 0.017	0.025	0.023	43
V	17.484 ± 0.029	$+0.029 \pm 0.003$	0.149 ± 0.015	0.019	0.018	36
S	16.611 ± 0.030	$+0.028 \pm 0.004$	0.078 ± 0.025	0.018	0.018	32

worth noting that Oliveira *et al.* (2013) reported higher values of 0.53 ± 0.05 mag for Sagar *et al.*'s (2001) data and 0.50 ± 0.02 mag for that of Kjeldsen and Frandsen (1991). Dias *et al.* (2012) reported 0.33 ± 0.03 mag, using 2MASS data.

Given the widespread and large uncertainties of these studies, it seemed worthwhile to contribute these old observations of Melotte 105 to the literature, particularly given the novel aspect that the Vilnius photometric system was used and estimates for spectral types could be made. The data collected for the current study were some of the first CCD imaging using this system (see Boyle *et al.* 1990a, b, 1992, 1996) and indeed were partly collected to test that useful data could be obtained using the system, by the then available telescopes in New Zealand, and then recently set up data reduction pathway described below.

3. Observations

Observations were made with the 1-m McLellan telescope at MJUO (Mount John University Observatory, New Zealand), using a cryogenically-cooled Thomson TH7882 CDA charge-coupled device. Images were collected using the photometrics PM-3000 computer running FORTH (Moore 1974) software with extensive local modifications, and written to half inch 9 track magnetic tape for transportation back to Victoria University of Wellington (VUW, New Zealand) for analysis. Images from these tapes were then converted into the FITS (Wells *et al.* 1981) format from the native photometrics one, and read into the Image Reduction and Analysis Facility (IRAF), where subsequent reduction took place. Details on the data pathway and image processing facility established at VUW are in Banks (1993). Further, details on the MJUO CCD data acquisition system and its characteristics may be found in Tobin (1992).

Melotte 105 was observed on February 15th 1994. Seeing was reasonable for MJUO, with a mean of 3.0 arcsecs for frames of the cluster. All exposures were 14.35 minutes long. The Vilnius filters were of different thicknesses, so flats had been attached to bring them all to the same optical depth (so that refocusing the telescope was not necessary). The U, P, X, Y, Z, V, and S filters used by this study are 9.79, 4.52, 3.26, 6.25, 6.64, 6.79 and 5.91 mm thick respectively. Schott FK5 was used for the P and X filters, and 8270 for the remainder, with careful attention paid to not significantly altering the spectral profiles of the filters. Dow Corning Q2-3067 optical couplant was used to attach suitably thick, pitch polished flats to the filters. During the observing run, air bubbles increasingly invaded the optical couplant of the Y filter, making it unsuitable for imaging. The lack of Y observations meant that the standard reduction technique for Vilnius data could not be followed for Melotte 105, as it centres around the Y filter. This method is described in Straižys and Sviderskienė (1972) and Straižys (1992a).

Standard stars were observed in NGC 4755. The IRAF "Fitparam" task was used to fit equations of the form:

$$M_{\rm o} = M + m_1 + (m_2 \times (X - V)) + (m_3 \times \text{air mass}), \quad (1)$$

where the subscript 'o' indicates the observational magnitudes, m are the coefficients and M the 'standard' magnitude. The coefficients of fits and their root mean squares (RMS) may be found in Table 1. Extinction and

instrumental coefficients were determined by the IRAF "photcal" package using a least-squares solution to all the standard star data (see Harris *et al.* 1981).

Aperture corrections add further uncertainties to the transformations, beyond those given in Table 1. The uncertainties in the aperture corrections for the U, P, X, Z, V and S filters are 0.029, 0.034, 0.013, 0.014, 0.008 and 0.024 magnitudes, respectively.

Three of Sher's (1965) stars, measured with photoelectric photometry were in common with the current study. Agreement was good for the stars. The V magnitudes were (12.09, 13.00, 14.08) in Sher compared to the present study of (11.96, 12.95, 14.01), while $X - V$ colours were (2.69, 0.99, 1.16) compared to (2.71, 0.92, 1.09). The relation given by Forbes (1996) was used to convert the $B - V$ colour to $X - V$.

4. Results

IRAF and its implementation of *DAOphot* (Stetson 1987) were used to reduce the CCD images. Further information on the processing steps followed may be found in Banks (1993), such as flat fielding and bias removal.

4.1 *Photometry*

The cluster has galactic coordinates (l, b)=(292°.90, –2°.41), and is therefore subject to substantial interstellar absorption. Reddening was estimated using a $P - X$, $Z - S$ colour–colour diagram as outlined by (Straižy 1992b). Colour excess $E(Z - S)$ is estimated as 0.32 ± 0.04 magnitudes, which corresponds to $E(B - V)$ being 0.34 ± 0.04. This value is within error of that of Sher (1965), but substantially different from the value given by Kjeldsen and Frandsen (1991). Santos (1993) estimated the reddening for Melotte 105 using integrated spectra of cluster stars in the visible and infrared as $E(B - V) = 0.30 \pm 0.02$ magnitudes, which is within the formal error of the reddening estimated by the present study. The reddening was used in conjunction with the expected luminosity class V sequence to estimate the distance modulus of the cluster. The true distance modulus $V - M_V$ was found to be 12.9 ± 0.3, which is again closer to the value given by Sher (1965), although with large uncertainty to the extent that it also overlaps with that of Kjeldsen and Frandsen (1991). Paunzen and Netopil (2006) reported a distance modulus of 11.8 (+0.43, –0.53), Monteiro *et al.* (2010) reported a distance modulus of 11.92 (+0.16, –0.17) and Yadav and Sagar (2002) reported a distance modulus of 12.07 (+0.08, –0.09) magnitudes — somewhat lower than this study's value.

Given the lack of Y observations, the standard classification technique outlined by Straižys (1992a); Straižy (1992b) could not be followed. However, Straižys (1974) proposed a technique based on the reddening-free energy distributions, i.e., using the so-called Q factors. This method could be used despite no Y data being available. The Q parameters were calculated with respect to the $V - S$ colour index. The parameters Q_{UVS}, Q_{PVS}, Q_{XVS} and Q_{ZVS} were then plotted against the central wavelength of the first filter in each Q factor. Normally, Q_{YVS} is included. These Q functions have very different shapes for different spectral types and luminosity classes.

While this "poor man's spectroscopy" did not require the Y filter, the effectiveness of the technique was reduced without it. In addition, only the brightest stars in the cluster could be classified, given that the exposures in each filter were of the same length. Hence the U and P filters had brighter limiting magnitudes, given their through-puts. The supergiants were classified as late G stars, while the main sequence extended from ∼B9 through to late A. The magnitudes, positions and identification numbers of the classified stars are given in Table 2. The table is sorted in order of increasing V magnitude. The errors given are those calculated by IRAF *DAOphot*. The stars with unusual classifications appear to be field stars, located on the CMDs well off the main sequence of the cluster (see Figure 1). The major problem with the technique was that the Q_λ functions for most of the spectral range (early to mid A stars) covered by the main sequence do not change greatly, especially given the missing Q_{YVS} factor. The $V \times X - V$ colour–magnitude diagram was therefore used to select the appropriate spectral type, and so the initial colour excess ratios, in the first iteration of the classification. At least two iterations were used to produce the results listed in the table (see also Figure 2). More were required for the unusual stars. Excesses for later iterations were based on the spectral type estimated by the immediately previous step.

The classifications are in good agreement with Frandsen *et al.* (1989) who commented that the main sequence for Melotte 105 commenced at B8. Kjeldsen and Frandsen (1991) stated that Sher (1965) reached down to the spectral type A5 on the main sequence. The faintest magnitude tabulated by Sher (1965) is 14.99, which corresponds to A5 V stars in the current analysis.

Table 2. Derived photometric values for Melotte 105. Each of the Vilnius magnitudes is given (U, P, X, Z, V, S) along with the photometric errors (dU, dP, dX, dZ, dV, dS), position on the CCD frame (x and y), identification number assigned by this study (ID), and the derived classification (Class).

U	dU	P	dP	X	dX	Z	dZ	V	dV	S	dS	x	y	ID	Class
16.41	0.02	15.48	0.01	14.50	0.01	12.25	0.03	11.89	0.03	10.88	0.04	203	238	184	G8I
14.65	0.01	13.65	0.01	12.75	0.01	12.10	0.01	11.89	0.01	11.40	0.01	154	258	201	B8III
14.79	0.01	13.71	0.01	12.81	0.01	12.13	0.03	11.91	0.02	11.38	0.01	114	314	258	B8III
16.48	0.01	15.64	0.01	14.62	0.01	12.41	0.01	11.96	0.02	11.06	0.02	26	198	139	G8I
16.42	0.02	15.52	0.01	14.69	0.01	12.57	0.01	12.15	0.01	11.23	0.01	303	437	358	G5I
15.08	0.01	14.10	0.01	13.15	0.01	12.59	0.01	12.35	0.01	12.16	0.05	116	170	116	NA
15.17	0.01	14.22	0.01	13.39	0.01	12.62	0.01	12.41	0.01	12.04	0.01	189	244	190	B9V
15.08	0.01	14.11	0.01	13.16	0.01	12.86	0.01	12.44	0.01	11.52	0.03	120	172	117	NA
15.13	0.01	14.15	0.01	13.36	0.01	12.63	0.01	12.44	0.01	12.06	0.01	272	354	296	B8V
15.39	0.01	14.46	0.01	13.57	0.01	12.79	0.01	12.57	0.01	12.17	0.01	82	321	266	B9V
15.59	0.01	14.57	0.01	13.68	0.01	12.87	0.01	12.65	0.01	12.25	0.01	186	314	259	B9V
15.57	0.01	14.60	0.01	13.71	0.01	12.93	0.01	12.70	0.01	12.31	0.01	181	232	177	B9V
15.53	0.02	14.55	0.01	13.73	0.01	12.97	0.01	12.74	0.01	12.34	0.01	249	241	188	B9V
15.49	0.01	14.60	0.01	13.68	0.01	12.96	0.01	12.75	0.01	12.35	0.01	86	63	33	B9V
15.58	0.01	14.60	0.01	13.78	0.01	13.01	0.01	12.81	0.01	12.41	0.01	239	363	302	B9V
16.98	0.02	16.11	0.01	15.23	0.01	13.28	0.01	12.85	0.01	11.96	0.01	147	223	166	K0III
15.57	0.01	14.63	0.01	13.86	0.01	13.14	0.01	12.97	0.01	12.61	0.01	227	440	360	B8V
15.87	0.01	14.91	0.01	14.03	0.01	13.22	0.01	13.00	0.01	12.60	0.01	57	414	340	B9V
15.59	0.01	14.71	0.01	13.93	0.01	13.20	0.01	13.01	0.01	12.69	0.01	284	412	339	A0V
15.83	0.01	14.84	0.01	14.00	0.01	13.24	0.01	13.03	0.01	12.66	0.01	273	315	260	B9V
16.09	0.01	15.10	0.01	14.28	0.01	13.30	0.01	13.07	0.01	12.61	0.02	342	547	415	B9V
16.06	0.01	15.04	0.01	14.24	0.01	13.46	0.01	13.27	0.01	12.88	0.01	162	427	350	B9V
16.32	0.02	15.37	0.01	14.42	0.01	13.53	0.01	13.30	0.01	12.88	0.01	69	395	326	A0V
15.95	0.01	15.11	0.01	14.25	0.01	13.52	0.01	13.32	0.01	12.96	0.01	225	147	97	B9V
16.13	0.01	15.24	0.01	14.33	0.01	13.54	0.01	13.33	0.01	12.94	0.01	54	207	145	A0V
16.14	0.02	15.34	0.02	14.43	0.01	13.53	0.01	13.34	0.01	12.87	0.02	204	184	127	B9V
16.18	0.01	15.31	0.01	14.41	0.01	13.62	0.01	13.42	0.01	13.06	0.01	120	219	148	A0V
16.21	0.01	15.32	0.01	14.49	0.01	13.71	0.01	13.49	0.01	13.10	0.01	178	302	246	B9V
16.08	0.01	15.20	0.01	14.44	0.01	13.72	0.01	13.52	0.01	13.18	0.01	331	265	216	B9V
16.29	0.02	15.46	0.02	14.60	0.01	13.84	0.01	13.56	0.01	13.23	0.01	210	228	171	A0V
16.39	0.02	15.44	0.01	14.57	0.01	13.77	0.01	13.56	0.01	13.19	0.01	216	381	316	A0V
16.51	0.02	15.62	0.01	14.71	0.01	13.94	0.01	13.73	0.01	13.35	0.01	61	340	283	B9V
16.48	0.01	15.58	0.01	14.77	0.01	13.95	0.01	13.75	0.01	13.36	0.01	301	393	325	B9V
16.53	0.02	15.65	0.01	14.80	0.01	13.95	0.01	13.77	0.01	13.29	0.01	127	263	211	B9V
16.66	0.02	15.76	0.01	14.81	0.01	14.01	0.01	13.80	0.01	13.44	0.01	98	149	100	A0V
16.78	0.02	15.82	0.01	14.88	0.01	14.09	0.01	13.88	0.01	13.52	0.01	99	165	110	A2V
16.63	0.02	15.91	0.01	14.97	0.01	14.16	0.01	13.97	0.01	13.60	0.01	162	86	52	A0V
16.87	0.02	15.97	0.01	15.09	0.01	14.22	0.01	14.00	0.01	13.65	0.01	278	298	242	A0V
17.06	0.02	16.12	0.02	15.19	0.01	14.27	0.02	14.01	0.02	13.58	0.02	152	218	158	A0V
16.97	0.02	16.08	0.01	15.09	0.01	14.24	0.01	14.02	0.01	13.63	0.01	20	131	84	A0V
17.00	0.02	16.08	0.01	15.21	0.01	14.23	0.01	14.02	0.01	13.62	0.01	54	523	403	A0V
17.39	0.04	16.58	0.02	16.02	0.01	14.39	0.01	14.04	0.01	13.69	0.01	151	403	330	G8IV
16.88	0.01	16.05	0.01	15.11	0.01	14.27	0.01	14.07	0.01	13.71	0.01	180	157	106	A2V
16.92	0.02	16.00	0.01	15.15	0.01	14.27	0.01	14.07	0.01	13.68	0.01	322	362	301	A0V
16.98	0.04	16.38	0.02	15.45	0.01	14.41	0.01	14.13	0.01	13.71	0.01	134	215	149	NA
17.09	0.03	16.13	0.02	15.21	0.01	14.38	0.01	14.15	0.01	13.77	0.01	162	415	342	A0V
17.27	0.03	16.33	0.02	15.47	0.01	14.39	0.01	14.15	0.01	13.70	0.01	92	328	271	A0V

Table 2. *Continued.*

U	dU	P	dP	X	dX	Z	dZ	V	dV	S	dS	x	y	ID	Class
17.35	0.03	16.49	0.02	15.82	0.01	14.50	0.01	14.16	0.01	13.50	0.01	44	376	311	K0VI
17.20	0.02	16.24	0.02	15.35	0.01	14.40	0.01	14.18	0.01	13.75	0.01	117	471	379	A2V
17.09	0.03	16.26	0.02	15.31	0.01	14.44	0.01	14.22	0.01	13.79	0.01	69	230	176	A5V
17.12	0.03	16.28	0.02	15.34	0.01	14.44	0.01	14.22	0.01	13.84	0.01	171	292	236	A0V
17.41	0.02	16.57	0.02	15.98	0.01	14.60	0.01	14.27	0.01	13.60	0.01	315	542	412	K2V
18.86	0.11	18.16	0.07	17.15	0.03	14.80	0.01	14.27	0.01	13.26	0.02	214	81	47	K0III
17.11	0.03	16.29	0.02	15.36	0.01	14.51	0.01	14.29	0.01	13.93	0.01	221	170	115	A2V
17.31	0.03	16.37	0.03	15.44	0.01	14.55	0.01	14.31	0.01	13.96	0.01	80	153	102	NA
17.31	0.03	16.46	0.02	15.58	0.01	14.56	0.01	14.31	0.01	13.93	0.01	103	316	269	A5V
17.45	0.03	16.44	0.02	15.55	0.01	14.50	0.01	14.39	0.01	13.98	0.01	143	283	227	A5V
17.33	0.03	16.46	0.02	15.52	0.01	14.60	0.01	14.40	0.01	14.04	0.01	13	377	310	A5V
17.23	0.03	16.46	0.02	15.50	0.01	14.65	0.01	14.43	0.01	14.07	0.01	248	183	128	A2V
17.32	0.03	16.45	0.04	15.74	0.01	14.74	0.01	14.44	0.01	13.99	0.01	227	232	179	A5V
17.36	0.03	16.60	0.02	15.62	0.01	14.70	0.01	14.47	0.01	14.05	0.01	131	105	62	A5V
17.52	0.03	16.75	0.02	15.73	0.01	14.78	0.01	14.55	0.01	14.15	0.01	39	80	46	A2V
17.63	0.03	16.70	0.02	15.84	0.01	14.83	0.01	14.58	0.01	14.21	0.01	116	489	387	NA
17.58	0.03	16.70	0.03	15.82	0.01	14.83	0.01	14.60	0.01	14.16	0.01	265	472	380	A0V
17.67	0.04	16.81	0.02	15.86	0.01	14.77	0.01	14.60	0.01	14.18	0.01	163	220	162	A5V
17.64	0.04	16.73	0.03	15.82	0.01	14.82	0.01	14.62	0.01	14.20	0.01	92	338	281	A5V
17.58	0.04	16.71	0.03	15.84	0.01	14.89	0.01	14.63	0.01	14.24	0.01	218	185	130	A2V
17.59	0.03	16.77	0.03	15.85	0.01	14.86	0.01	14.63	0.01	14.22	0.01	219	216	157	A5V
17.50	0.04	16.72	0.02	15.84	0.01	14.89	0.01	15.65	0.01	14.24	0.01	294	71	39	A5V
17.66	0.03	16.74	0.02	15.87	0.01	14.87	0.01	14.65	0.01	14.22	0.01	208	269	217	A5V
17.78	0.05	17.14	0.03	16.48	0.02	15.02	0.01	14.65	0.01	13.97	0.01	52	44	15	K4V
17.66	0.04	16.96	0.05	16.38	0.05	15.08	0.06	14.68	0.06	13.94	0.03	317	221	164	G2V
17.74	0.04	16.76	0.03	15.95	0.01	14.99	0.01	14.74	0.01	14.33	0.01	279	250	193	A5V
17.86	0.04	16.88	0.02	15.95	0.01	14.99	0.01	14.75	0.01	14.36	0.01	124	384	318	A5V
17.65	0.03	16.85	0.02	16.00	0.01	15.01	0.01	14.76	0.01	14.34	0.01	285	178	123	A5V
17.87	0.05	17.04	0.04	16.04	0.02	15.06	0.01	14.76	0.03	14.42	0.02	171	310	254	NA
17.79	0.04	16.95	0.03	16.01	0.01	15.01	0.01	14.78	0.01	14.36	0.01	157	375	308	A5V
17.68	0.03	16.97	0.02	16.05	0.01	15.06	0.01	14.82	0.01	14.39	0.01	252	107	65	A5V
17.74	0.03	17.01	0.03	16.32	0.01	15.11	0.01	14.82	0.01	14.26	0.01	333	105	64	F0V
17.88	0.04	16.99	0.03	16.20	0.01	15.04	0.02	14.82	0.02	14.40	0.02	210	245	191	A5V
17.87	0.04	17.05	0.03	16.12	0.01	15.11	0.01	14.85	0.01	14.42	0.01	208	286	234	A5V
17.98	0.05	17.12	0.04	16.17	0.01	15.17	0.01	14.88	0.01	14.46	0.01	44	202	143	A5V
17.86	0.04	16.99	0.02	16.14	0.01	15.16	0.01	14.91	0.01	14.51	0.01	268	234	182	A5V
17.83	0.04	17.01	0.04	16.33	0.03	15.22	0.03	14.95	0.02	14.55	0.01	294	282	226	A5V
18.04	0.04	17.04	0.03	16.25	0.01	15.21	0.01	14.96	0.01	14.55	0.01	236	534	407	K1IV
18.17	0.06	17.17	0.03	16.30	0.01	15.28	0.01	15.02	0.01	14.63	0.01	123	357	298	A5V
17.32	0.06	16.44	0.04	16.36	0.01	15.26	0.01	15.05	0.01	14.59	0.01	231	235	183	NA
18.27	0.07	17.27	0.03	16.40	0.02	15.32	0.01	15.05	0.01	14.60	0.01	108	256	200	A5V
18.03	0.05	17.22	0.04	16.33	0.01	15.34	0.01	15.06	0.01	14.63	0.01	237	259	207	A5V
18.28	0.07	17.40	0.03	16.53	0.01	15.36	0.01	15.07	0.01	14.60	0.01	194	213	153	A5V
18.24	0.05	17.29	0.03	16.44	0.01	15.39	0.01	15.12	0.01	14.71	0.01	283	465	376	A5V
18.25	0.05	17.49	0.05	16.71	0.03	15.43	0.03	15.17	0.03	14.47	0.04	301	75	43	F5V
18.41	0.06	17.45	0.03	16.64	0.02	15.49	0.01	15.19	0.01	14.78	0.01	203	321	267	NA
18.58	0.08	17.46	0.03	16.64	0.02	15.54	0.01	15.28	0.01	14.89	0.02	145	233	181	NA
18.33	0.05	17.53	0.04	16.63	0.02	15.57	0.01	15.29	0.01	14.82	0.01	97	176	119	A5V
18.41	0.07	17.44	0.04	16.71	0.02	15.62	0.01	15.32	0.01	14.83	0.01	339	342	288	A7V

Table 2. *Continued.*

U	dU	P	dP	X	dX	Z	dZ	V	dV	S	dS	x	y	ID	Class
18.43	0.06	17.63	0.05	16.73	0.02	15.59	0.01	15.33	0.01	14.86	0.01	95	208	147	A5V
18.38	0.07	17.52	0.04	16.81	0.02	15.63	0.01	15.40	0.01	14.91	0.01	185	541	411	A7V
18.43	0.07	17.56	0.04	16.79	0.01	15.68	0.01	15.40	0.01	14.93	0.01	245	342	287	A7V
18.37	0.06	17.57	0.04	17.07	0.02	15.79	0.01	15.46	0.01	14.86	0.01	316	298	243	F0V
18.75	0.08	17.69	0.04	17.08	0.02	15.86	0.02	15.53	0.02	15.08	0.02	301	413	341	NA
18.39	0.05	17.81	0.05	17.23	0.03	15.96	0.02	15.59	0.01	14.98	0.01	354	62	32	F2V
18.68	0.08	17.65	0.04	17.07	0.02	15.94	0.01	15.61	0.01	15.09	0.01	331	251	194	F0V
19.32	0.21	18.06	0.07	17.83	0.03	16.03	0.01	15.69	0.02	15.12	0.01	162	241	187	NA
18.60	0.08	17.89	0.05	17.18	0.02	16.01	0.01	15.71	0.01	15.16	0.01	325	335	279	F0V
18.94	0.11	18.08	0.07	17.40	0.03	16.05	0.03	15.71	0.04	15.39	0.01	270	134	91	NA
18.81	0.09	17.86	0.06	17.25	0.03	16.04	0.01	15.72	0.01	15.15	0.01	296	102	59	A7V
18.64	0.08	18.03	0.06	17.49	0.03	16.08	0.02	15.74	0.02	15.18	0.01	103	58	26	A7V
18.80	0.11	18.19	0.06	17.49	0.03	16.12	0.02	15.78	0.01	15.13	0.01	19	62	31	F0V
19.01	0.10	18.24	0.07	17.40	0.03	16.18	0.01	15.88	0.01	15.29	0.01	196	347	293	A7V
19.25	0.16	18.43	0.08	17.65	0.03	16.34	0.02	15.96	0.02	15.37	0.01	43	333	277	NA
19.10	0.17	18.25	0.06	17.58	0.03	16.29	0.02	16.01	0.01	15.43	0.02	115	548	416	A7V
18.89	0.09	18.24	0.07	17.71	0.03	16.46	0.01	16.09	0.01	15.51	0.01	362	154	103	F2V
18.77	0.10	18.50	0.09	17.70	0.03	16.45	0.01	16.14	0.01	15.53	0.01	265	483	385	F0V
19.50	0.17	18.66	0.10	17.90	0.03	16.49	0.03	16.24	0.03	15.68	0.02	299	314	261	NA
18.79	0.08	17.96	0.07	17.66	0.05	16.21	0.04	16.67	0.41	16.04	0.04	332	6	2	NA

4.2 *GAIA data*

We compiled the *Gaia* DR2 photometric and astrometric catalog of the observation results of Melotte 105 determined by Vilnius photometry. For this, we matched the star chart of the cluster with *Gaia* DR2's equatorial coordinates (α_{2000}, δ_{2000}), to obtain the photometric data (G magnitude and $BP-RP$ colour), trigonometric parallaxes (ϖ), proper motion components ($\mu_\alpha \cos\delta$, μ_δ) and their errors of the stars located through the region of Melotte 105. However, the astrometric data of three of the 116 stars in the catalog is not available. We listed photometric and astrometric *Gaia* DR2 data of the cluster in Table 3.

4.3 *Structural parameters of the cluster*

We constructed the Radial Density Profile (RDP) of Melotte 105 to investigate its structural parameters. The central equatorial coordinates of the cluster ($\alpha_{2000} = 11^{\rm h}\,19^{\rm m}\,42^{\rm s}$, $\delta_{2000} = -63^\circ\,29'00''$) were taken from SIMBAD database.[1] Taking into account these coordinates, we calculated the number density of stars which are located in 0.5 arcmin-wide concentric circles centered from the cluster center to 3.5 arcmin. Then we fitted the RDP with a model by King (1962) and obtained the cluster's central stellar density $f_0 = 13.472 \pm 0.219$ star/arcmin^2, background stellar density $f_{\rm bg} = 0.550 \pm 0.292$ star/arcmin^2, and core radius $r_{\rm c} = 1.392 \pm 0.066$ arcmin. The RDP presented in Figure 3 indicates that most of the stellar density of the cluster is within 3.5 arcmin.

4.4 *Cluster membership and CMDs*

To define precise astrophysical parameters of Melotte 105, one should clean the field star contamination from the cluster member stars. In most cases, colour–magnitude diagrams (CMDs) of clusters are insufficient to separate field stars from the cluster stars. For those cases, there are some statistical methods that take into account the proper motion values of the stars (Ak *et al.* 2016; Krone-Martins and Moitinho 2014; Javakhishvili *et al.* 2006; Balaguer-Nunez *et al.* 1998) to calculate membership probabilities of stars, determining whether the stars are components of the the cluster or not.

In this study, we used $UPXZVS$ Vilnius magnitude, colours and *Gaia* DR2 astrometric data ($\mu_\alpha \cos\delta$, μ_δ and ϖ) and utilized a statistical method called UPMASK (Unsupervised Photometric Membership Assignment in Stellar Clusters, Krone-Martins and

[1] http://simbad.u-strasbg.fr/simbad/sim-fbasic.

Table 3. Gaia DR2 data for the stars in the direction of the Melotte 105: ID is the identification assigned to a star by this study, α is the right ascension, δ is the declination, 'Gmag' the *Gaia* magnitude, 'Plx' the parallax, ϵ(Plx) the error in the parallax, $\alpha_{\rm pm}$ is the right ascension proper motion, $\epsilon(\alpha_{\rm pm})$ is the error in the right ascension proper motion, $\delta_{\rm pm}$ is the declination proper motion, $\epsilon(\delta_{\rm pm})$ the error in the declination proper motion, and 'Prob' is the probability of cluster membership derived by this study. BP stands for the *Gaia* Blue Photometer, which operates in the wavelength range 330–680 nm. RP stands for the *Gaia* Red Photometer, which covers the wavelength range 640–1050 nm, hence 'BP–RP' is the colour difference between these two filters.

ID	α	δ	Gmag	BP–RP	Plx	ϵ(Plx)	$\alpha_{\rm pm}$	$\epsilon(\alpha_{\rm pm})$	$\delta_{\rm pm}$	$\epsilon(\delta_{\rm pm})$	Prob
184	11:19:36.94	−63:29:11.27	11.316	1.679	0.3843	0.0282	−6.750	0.050	2.150	0.045	0.97
201	11:19:41.54	−63:28:59.15	11.812	0.658	0.1348	0.0509	−6.120	0.085	1.897	0.073	0.00
258	11:19:45.29	−63:28:24.61	11.758	0.710	0.4109	0.0262	−6.755	0.042	1.978	0.045	0.99
139	11:19:53.28	−63:29:36.79	11.549	1.649	0.4444	0.0331	−6.716	0.051	2.186	0.048	0.97
358	11:19:27.95	−63:27:07.18	11.802	1.593	0.4151	0.0263	−6.885	0.042	2.192	0.043	0.98
116	11:19:45.07	−63:29:53.10	12.282	0.622	0.4037	0.0315	−6.903	0.055	2.088	0.066	0.98
190	11:19:38.29	−63:29:07.40	12.383	0.654	0.4038	0.0280	−6.717	0.046	2.136	0.043	0.95
117	11:19:44.73	−63:29:52.64	12.282	0.622	0.4037	0.0315	−6.903	0.055	2.088	0.066	0.95
296	11:19:30.72	−63:27:58.82	12.425	0.594	0.4280	0.0281	−6.890	0.045	2.095	0.047	0.95
266	11:19:48.25	−63:28:20.62	12.506	0.660	0.3818	0.0290	−6.722	0.047	2.597	0.048	0.47
259	11:19:38.59	−63:28:23.82	12.594	0.701	0.3613	0.0284	−6.737	0.045	2.056	0.048	0.97
177	11:19:39.07	−63:29:14.80	12.651	0.669	0.3764	0.0298	−6.735	0.052	2.308	0.054	0.84
188	11:19:32.69	−63:29:08.76	12.686	0.645	0.4118	0.0289	−6.786	0.049	2.190	0.045	0.97
33	11:19:47.76	−63:30:58.31	12.751	0.614	0.4192	0.0280	−6.880	0.040	2.080	0.040	0.99
302	11:19:33.81	−63:27:53.67	12.760	0.650	0.4897	0.0307	−6.938	0.048	2.199	0.047	0.97
166	11:19:42.10	−63:29:21.51	12.530	1.549	–	–	–	–	–	–	0.00
360	11:19:35.01	−63:27:05.67	12.942	0.544	0.4318	0.0228	−6.874	0.034	2.261	0.037	1.00
340	11:19:50.75	−63:27:23.00	12.941	0.653	0.4136	0.0206	−6.767	0.033	2.083	0.031	1.00
339	11:19:29.66	−63:27:22.40	12.997	0.534	0.4301	0.0208	−6.803	0.033	2.068	0.032	1.00
260	11:19:30.56	−63:28:22.98	13.015	0.633	0.3503	0.0204	−6.748	0.033	2.036	0.033	0.95
415	11:19:24.68	−63:25:57.27	13.010	0.777	0.5366	0.0233	−9.468	0.034	3.383	0.036	0.32
350	11:19:41.06	−63:27:13.90	13.226	0.615	0.4074	0.0179	−6.749	0.030	1.842	0.028	0.81
326	11:19:49.53	−63:27:35.06	13.249	0.722	0.6299	0.0166	−4.543	0.027	1.764	0.026	0.22
97	11:19:34.79	−63:30:07.11	13.316	0.557	0.3940	0.0173	−6.890	0.020	1.940	0.020	0.87
145	11:19:50.66	−63:29:30.99	13.283	0.639	0.4004	0.0187	−7.267	0.029	2.179	0.029	0.53
127	11:19:36.93	−63:29:44.20	13.464	0.691	–	–	–	–	–	–	0.00
148	11:19:44.63	−63:29:29.66	13.384	0.613	0.4041	0.0183	−6.618	0.032	2.003	0.031	0.88
246	11:19:39.48	−63:28:31.20	13.460	0.631	0.3894	0.0172	−6.710	0.028	1.837	0.027	0.76
216	11:19:25.28	−63:28:51.00	13.504	0.539	0.3833	0.0169	−6.723	0.026	2.197	0.026	0.97
171	11:19:36.37	−63:29:17.10	13.552	0.646	0.4219	0.0208	−6.822	0.034	2.078	0.032	0.97
316	11:19:36.01	−63:27:42.10	13.512	0.636	0.4043	0.0186	−6.972	0.029	2.047	0.030	0.98
283	11:19:50.24	−63:28:08.40	13.670	0.620	0.3774	0.0201	−6.565	0.031	2.248	0.029	0.85
325	11:19:28.08	−63:27:34.21	13.704	0.632	0.3851	0.0223	−6.753	0.032	1.980	0.031	0.96
211	11:19:44.11	−63:28:55.30	13.650	0.679	0.4379	0.0188	−6.759	0.030	2.055	0.035	0.95
100	11:19:46.52	−63:30:06.87	13.779	0.610	0.4375	0.0198	−6.807	0.032	2.032	0.030	1.00
110	11:19:46.55	−63:29:56.60	13.855	0.620	0.4258	0.0229	−6.761	0.038	2.166	0.039	0.98
52	11:19:40.56	−63:30:45.07	13.948	0.631	0.4702	0.0222	−6.540	0.030	2.200	0.030	0.97
242	11:19:30.19	−63:28:33.40	13.981	0.679	0.5363	0.0216	−6.966	0.032	2.307	0.032	0.90
158	11:19:41.74	−63:29:23.50	14.075	0.704	0.3468	0.0252	−6.796	0.039	2.319	0.041	0.99
84	11:19:53.70	−63:30:18.69	13.991	0.675	0.3954	0.0199	−6.740	0.030	2.180	0.030	0.98
403	11:19:51.07	−63:26:14.10	13.979	0.710	0.5436	0.0209	−4.447	0.032	0.167	0.030	0.18
330	11:19:41.91	−63:27:29.44	13.818	1.313	1.0824	0.0244	2.941	0.040	−3.973	0.039	0.00
106	11:19:38.99	−63:30:01.33	14.022	0.629	0.3826	0.0205	−6.794	0.036	1.898	0.028	0.91

Table 3. *Continued.*

ID	α	δ	Gmag	BP–RP	Plx	ϵ(Plx)	α_{pm}	$\epsilon(\alpha_{pm})$	δ_{pm}	$\epsilon(\delta_{pm})$	Prob
301	11:19:26.14	−63:27:53.50	14.049	0.655	0.4006	0.0218	−6.729	0.033	2.037	0.038	0.99
149	11:19:43.37	−63:29:25.60	14.084	0.850	0.3968	0.0234	−6.715	0.035	1.934	0.038	0.99
271	11:19:47.35	−63:28:16.20	14.198	0.823	0.3420	0.0213	−6.683	0.033	2.080	0.033	0.77
342	11:19:40.95	−63:27:21.77	14.140	0.652	0.4086	0.0219	−6.783	0.037	2.028	0.034	0.96
311	11:19:51.81	−63:27:46.61	13.963	1.160	0.5115	0.0202	−14.180	0.034	3.393	0.032	0.23
379	11:19:45.32	−63:26:47.23	14.092	0.743	0.3908	0.0193	−6.371	0.030	1.842	0.031	0.32
176	11:19:49.39	−63:29:16.40	14.242	0.683	0.3410	0.0204	−6.747	0.035	2.122	0.036	0.93
236	11:19:39.92	−63:28:37.50	14.201	0.696	0.3586	0.0262	−6.985	0.043	2.172	0.035	0.96
47	11:19:35.88	−63:30:47.47	13.854	1.780	0.3622	0.0187	−9.230	0.020	2.860	0.020	0.41
412	11:19:27.10	−63:26:00.22	14.093	1.152	0.7124	0.0365	−11.390	0.057	3.411	0.055	0.19
115	11:19:35.18	−63:29:52.99	14.267	0.646	0.3843	0.0216	−6.668	0.035	2.188	0.030	0.99
102	11:19:48.30	−63:30:03.90	14.343	0.663	0.3305	0.0254	−6.897	0.042	2.111	0.039	0.91
269	11:19:46.29	−63:28:17.28	14.286	0.749	0.4296	0.0204	−6.854	0.032	2.098	0.034	0.96
227	11:19:42.59	−63:28:43.20	14.316	0.744	0.4349	0.0205	−6.720	0.034	2.146	0.032	0.95
310	11:19:54.65	−63:27:46.66	14.345	0.681	0.4030	0.0213	−6.722	0.035	2.104	0.038	1.00
128	11:19:32.69	−63:29:44.67	14.393	0.650	0.3917	0.0234	−6.708	0.035	2.193	0.033	0.96
179	11:19:34.87	−63:29:14.20	14.348	0.863	0.3861	0.0227	−6.692	0.036	2.219	0.032	0.96
62	11:19:43.47	−63:30:34.03	14.412	0.728	0.3836	0.0215	−6.760	0.030	2.200	0.030	1.00
46	11:19:51.54	−63:30:43.84	–	–	–	–	–	–	–	–	0.00
387	11:19:45.32	−63:26:34.59	14.545	0.760	0.4600	0.0217	−7.048	0.034	1.899	0.036	0.71
162	11:19:40.74	−63:29:21.90	14.512	0.806	0.3608	0.0320	−6.986	0.050	1.860	0.043	0.94
380	11:19:31.76	−63:26:45.41	14.519	0.766	0.3754	0.0227	−6.719	0.037	2.281	0.036	0.96
281	11:19:47.27	−63:28:09.65	14.555	0.801	0.4032	0.0225	−6.673	0.036	2.179	0.034	0.98
130	11:19:35.53	−63:29:43.71	14.571	0.757	0.4056	0.0239	−6.662	0.037	2.186	0.033	0.95
157	11:19:35.48	−63:29:24.76	14.570	0.763	0.3872	0.0251	−6.801	0.038	2.390	0.035	0.90
15	11:19:50.82	−63:31:11.54	14.505	1.185	1.1030	0.0206	−16.580	0.033	−0.338	0.032	0.00
217	11:19:36.62	−63:28:51.40	14.577	0.753	0.4033	0.0244	−6.774	0.037	2.040	0.036	0.96
164	11:19:26.53	−63:29:20.12	14.955	1.232	0.4912	0.0265	−7.624	0.042	−0.213	0.043	0.44
193	11:19:30.04	−63:29:02.50	14.686	0.722	0.3796	0.0250	−6.569	0.042	2.016	0.056	0.79
318	11:19:44.37	−63:27:40.98	14.662	0.740	0.3918	0.0229	−6.854	0.037	2.121	0.035	0.99
123	11:19:29.29	−63:29:47.41	14.689	0.769	0.3710	0.0236	−6.842	0.037	2.239	0.035	0.99
254	11:19:40.01	−63:28:26.86	14.807	0.755	0.4118	0.0259	−6.793	0.039	2.201	0.045	0.95
308	11:19:41.30	−63:27:46.80	14.679	0.757	0.4427	0.0244	−6.795	0.040	2.268	0.038	0.97
64	11:19:24.76	−63:30:32.50	14.719	0.953	0.4388	0.0240	−6.650	0.030	2.190	0.030	0.96
65	11:19:32.29	−63:30:31.39	14.748	0.775	0.4324	0.0242	−6.730	0.030	1.960	0.030	0.96
191	11:19:36.29	−63:29:06.31	14.795	0.801	0.4068	0.0254	−6.839	0.043	2.193	0.043	1.00
234	11:19:36.54	−63:28:40.33	14.752	0.796	0.3827	0.0273	−6.787	0.041	2.293	0.039	1.00
143	11:19:51.55	−63:29:34.11	14.824	0.814	0.3991	0.0281	−6.729	0.043	2.258	0.047	0.95
182	11:19:30.91	−63:29:13.19	14.822	0.747	0.4010	0.0282	−6.770	0.041	2.245	0.040	0.98
226	11:19:28.65	−63:28:43.20	14.983	0.810	0.3543	0.0269	−6.776	0.043	1.983	0.051	0.94
407	11:19:34.28	−63:26:06.88	14.886	0.796	0.4093	0.0262	−6.645	0.039	1.831	0.040	0.59
298	11:19:44.42	−63:27:58.21	14.911	0.797	0.4398	0.0303	−6.769	0.056	2.141	0.043	0.98
183	11:19:34.50	−63:29:12.20	14.946	0.830	0.4317	0.0267	−6.817	0.041	2.130	0.039	0.99
200	11:19:45.81	−63:29:00.00	14.944	0.859	0.3686	0.0268	−6.590	0.044	2.270	0.041	0.87
207	11:19:33.80	−63:28:57.55	14.940	0.779	0.4323	0.0272	−6.784	0.047	2.169	0.051	0.98
153	11:19:37.85	−63:29:26.10	14.928	0.920	0.4483	0.0254	−6.747	0.042	2.192	0.038	0.96
376	11:19:30.06	−63:26:49.61	15.028	0.809	0.4195	0.0272	−6.587	0.044	2.104	0.042	1.00
43	11:19:27.70	−63:30:51.53	15.250	1.072	0.2375	0.2339	−10.390	0.363	4.567	0.322	0.60
267	11:19:37.05	−63:28:19.58	15.139	0.884	0.4390	0.0298	−6.735	0.049	2.168	0.044	1.00
181	11:19:42.29	−63:29:14.22	15.059	0.894	0.4001	0.0269	−7.440	0.044	2.623	0.040	0.51

Table 3. *Continued.*

ID	α	δ	Gmag	BP–RP	Plx	ϵ(Plx)	α_{pm}	$\epsilon(\alpha_{pm})$	δ_{pm}	$\epsilon(\delta_{pm})$	Prob
119	11:19:46.64	−63:29:49.91	15.191	0.869	0.3579	0.0296	−6.967	0.051	2.150	0.050	0.90
288	11:19:24.47	−63:28:05.68	15.204	0.871	0.3937	0.0310	−6.555	0.048	2.115	0.046	0.92
147	11:19:46.87	−63:29:30.38	15.207	0.916	0.3967	0.0302	−6.948	0.049	1.956	0.059	0.95
287	11:19:33.19	−63:28:06.13	15.260	0.875	0.4013	0.0386	−6.819	0.052	2.163	0.050	0.96
411	11:19:39.13	−63:26:02.68	15.273	0.888	0.4496	0.0296	−6.871	0.045	2.257	0.047	0.95
243	11:19:26.68	−63:28:33.10	15.281	1.098	0.5288	0.0287	−7.622	0.046	2.032	0.050	0.07
341	11:19:28.22	−63:27:21.60	15.489	0.940	0.4169	0.0360	−6.634	0.054	2.098	0.051	0.97
32	11:19:22.92	−63:30:57.63	15.445	1.099	0.4736	0.0362	−6.550	0.050	2.480	0.040	0.86
194	11:19:25.12	−63:29:02.20	15.511	0.939	0.4688	0.0340	−6.564	0.053	2.159	0.050	1.00
39	11:19:28.50	−63:30:53.46	15.250	1.072	0.2375	0.2339	−10.390	0.363	4.567	0.322	0.29
187	11:19:40.67	−63:29:09.29	15.433	1.101	0.3932	0.0347	−6.471	0.062	2.224	0.048	0.96
91	11:19:30.66	−63:30:13.73	15.815	1.047	0.4044	0.0381	−6.710	0.060	2.360	0.050	0.93
279	11:19:25.84	−63:28:09.80	15.556	0.958	0.4100	0.0368	−6.876	0.056	1.981	0.055	0.85
59	11:19:28.28	−63:30:34.20	15.569	1.008	0.4677	0.0354	−6.690	0.050	1.980	0.040	0.88
26	11:19:46.14	−63:31:02.52	15.607	1.000	0.5296	0.0329	−6.770	0.050	2.160	0.040	0.95
31	11:19:53.79	−63:31:00.09	15.580	1.142	0.4031	0.0325	−6.530	0.050	2.220	0.040	0.97
293	11:19:37.73	−63:28:03.70	15.687	1.039	0.3921	0.0417	−6.729	0.060	2.066	0.060	0.98
277	11:19:51.77	−63:28:13.37	15.770	1.096	0.4285	0.0385	−6.621	0.060	2.208	0.058	0.96
416	11:19:45.50	−63:25:58.46	15.836	1.056	0.4587	0.0400	−6.737	0.061	2.213	0.061	0.96
103	11:19:22.30	−63:30:00.43	15.941	1.060	0.5180	0.0423	−6.423	0.068	2.154	0.061	0.98
385	11:19:31.58	−63:26:37.58	15.907	1.090	0.4668	0.0397	−6.683	0.064	2.197	0.061	0.97
261	11:19:28.22	−63:28:23.20	16.079	1.090	0.3947	0.0436	−6.744	0.070	2.156	0.065	0.96
2	11:19:24.62	−63:31:22.93	16.851	1.462	0.4119	0.0689	−10.260	0.100	4.180	0.090	0.33

Moitinho 2014) in order to calculate membership probabilities. The UPMASK method relies on minimal physical assumptions about high density stellar regions and is suitable for clusters 2–2.5 kpc from the Sun. We applied it to the five-dimensional astrometric space based on equatorial coordinates, proper motions and parallaxes of stars and four-dimensional photometric space ($V \times P - V$, $V \times X - V$, $V \times U - V$, $V \times Z - V$). We calculated the membership probabilities (P, not to be confused with the Vilnius filter) of the 116 stars located through Melotte 105 and showed their distribution on membership probability histogram (Figure 4). As shown in this figure, the membership probabilities of 99 of 116 stars are greater than $P = 0.5$, so these stars are adopted as most probable members of the Melotte 105 and used in further analysis. In fact, when the Vector Point Diagram (VPD) is examined (Figure 5), it is seen that stars with $P \geq 0.5$ are concentrated in a certain proper motion space. The red circles denote the most probable member stars $P \geq 0.5$ while open circles represent the low probable stars ($P < 0.5$) located through the cluster region. Intersection of the blue dashed lines represents the median proper motion values that are calculated from proper motions of 99 most probable cluster member stars. The median values of proper motion components are as follows: ($\langle \mu_\alpha \cos\delta \rangle = -6.753 \pm 0.041$, $\langle \mu_\delta \rangle = 2.156 \pm 0.040$ mas/yr). Next, we constructed CMDs of the Melotte 105 for four photometric colours ($V \times U - V$, $V \times X - V$, $V \times P - V$, $V \times Z - V$) and marked the stars with $P \geq 0.5$ on these diagrams (see Figure 6.) When we examine the figure by eye, it is seen that the main-sequence, turn-off point and giant stars can be distinguished. The turn-off points of CMDs contain stars whose apparent V magnitudes are between ∼11.5 and 13 mag, while evolved stars are bright ($V \sim 12$ mag) and they are in the red colour region (i.e. $X - V \sim 2.5$ mag) of the diagrams.

4.5 *Colour excess determination*

To calculate the colour excesses towards the cluster, we used the 84 main-sequence stars whose membership probabilities are $P \geq 0.5$ and with apparent magnitudes $V \geq 12$. The de-reddened ZAMS relations for Vilnius photometry are taken from Straižys (1992a). The two-colour diagrams (TCDs), $(P - V) \times (X - V)$ and $(U - V) \times (Z - V)$ were used to estimate the reddening (see Figure 7). The selective absorption

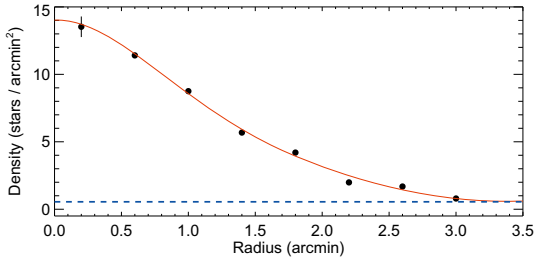

Figure 3. The radial density profile of the Melotte 105. The best-fit model is shown as the red solid line. Errors were determined as $1/\sqrt{N}$, where N indicates the number of stars used in density estimation. The blue dashed line represents the background stellar density for observational data.

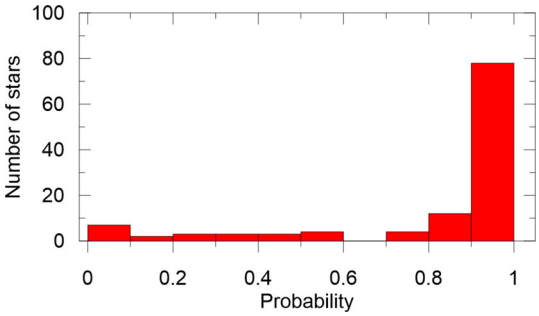

Figure 4. Membership probability as calculated by UPMASK. Stars with a probability greater than ≥ 0.5 are selected as cluster members by this study.

coefficients[2] for Vilnius photometry were taken from Munari and Fiorucci (2003) and used in the calculation of the reddening vectors. Based on these, the slopes of the reddening vectors were calculated as $\frac{E(P-V)}{E(X-V)} = 1.223$ and $\frac{E(U-V)}{E(Z-V)} = 7.901$ and used to adjust the position of the ZAMS on the TCDs. Minimum χ^2 fitting derived the following estimates of the colour excesses and their one-sigma intervals: $E(P-V) = 0.637 \pm 0.022$, $E(X-V) = 0.521 \pm 0.018$, $E(U-V) = 0.877 \pm 0.055$, and $E(Z-V) = 0.111 \pm 0.007$. Using the relation $E(X-V) = 1.285 \times E(B-V)$, we obtained $E(B-V) = 0.403 \pm 0.020$ magnitudes, which is larger than the estimate above $E(B-V) = 0.34 \pm 0.04$ mag although the two sigma intervals overlap. In passing, we note that the Q-factor method used above to calculate spectral type estimates is a reddening free technique (see Straižys 1974, who described it as a method "insensitive to interstellar reddening"), and so these estimates do not need to be recalculated based on this refined reddening estimate.

[2] $\frac{A_U}{A_V} = 1.621$, $\frac{A_P}{A_V} = 1.511$, $\frac{A_X}{A_V} = 1.419$, $\frac{A_Z}{A_V} = 1.082$, $\frac{A_{VIL}}{A_V} = 1.004$ and $A_V = 3.1 \times E(B-V)$.

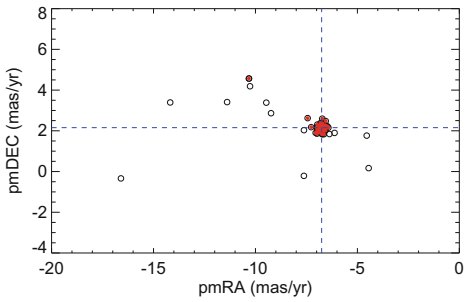

Figure 5. The vector point diagram for the observed stars: red circle denotes the most probable member stars, as per Figure 4. The intersection of two blue dashed lines presents the median proper motion values calculated from the proper motions of these 99 selected stars, as reported in the text.

4.6 *Age determination*

The age of Melotte 105 was determined by comparing the PARSEC isochrones (Bressan *et al.* 2012; Tang *et al.* 2014; Chen *et al.* 2014) for $Z = 0.025$ with the observed CMDs (see Figure 8). Metal abundance calibrations are sensitive to the Y band, which is unfortunately lacking in the Vilnius data set obtained by this study. We were therefore not able to determine the metal abundance of the cluster using the photometric metal abundance calibrations. Hence the metallicity of the cluster was not estimated via an independent method. For this reason, during age estimation of Melotte 105, the distance modulus and metallicity are derived simultaneously excluding reddening. We used PARSEC isochrones with different ages and metallicities to obtain the best-fit results to $V \times (P-V)$, $V \times (X-V)$, $V \times (U-V)$ and $V \times (Z-V)$ CMDs. To do this, we took into account the standard selective absorption coefficient as $R_V = 3.11$ for Vilnius photometric system (Munari & Fiorucci 2003). The uncertainties in age ($\Delta t = 25$ Myr) and distance ($\Delta\mu = 0.07$ mag) are suitable for the distribution of the most cluster member stars. The Z metal abundance was transformed to [Fe/H] using equations given by Bovy[3] who analytically obtained them using PARSEC isochrones (see also, Yontan *et al.* 2019; Bostancı *et al.* 2018; Bilir *et al.* 2016) and calculated the metallicity as [Fe/H]=0.24 dex. We represented the CMDs with the best-fit PARSEC isochrones in Figure 8 and the results were listed in Table 4. Melotte 105 is estimated to be 240 ± 25 Myr old. The cluster distance derived from the main-sequence fitting is 2078 ± 78 pc. We compare this with Bailer-Jones *et al.* (2018) who inferred distances to essentially all 1.33 billion

[3] https://github.com/jobovy/isodist/blob/master/isodist/Isochrone.py.

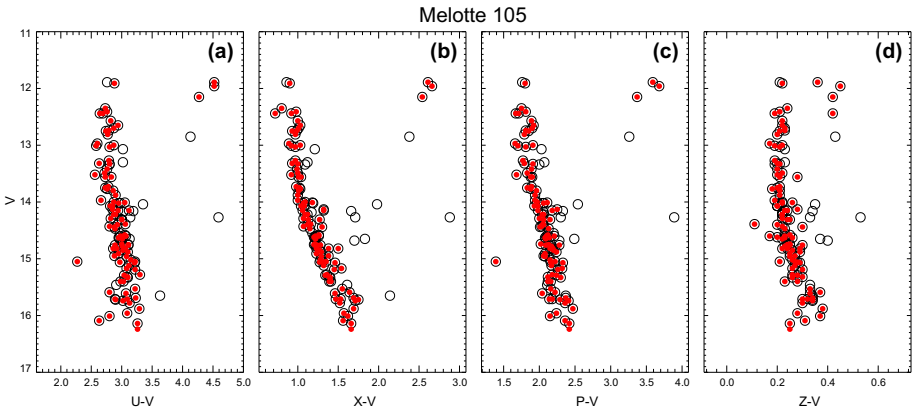

Figure 6. Vilnius colour-magnitude diagrams tagged with derived client membership: red circles denote the most probable member stars, as per Figure 4. Subplots are for **(a)** $U-V$, **(b)** $X-V$, **(c)** $P-V$ and **(d)** $Z-V$.

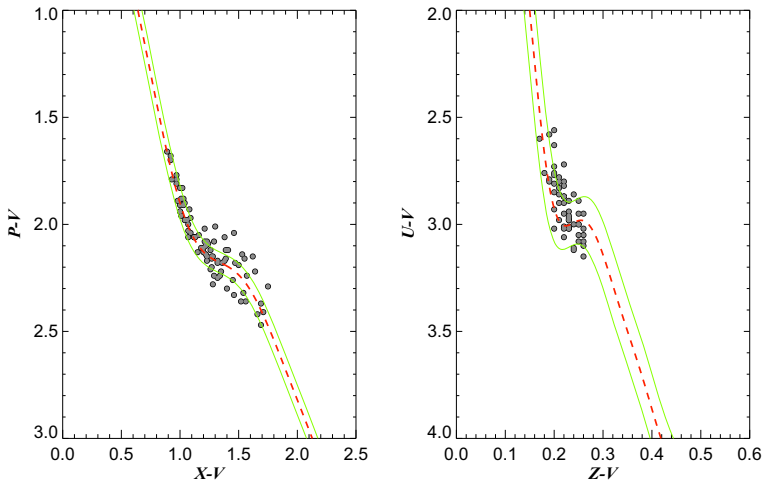

Figure 7. Two-colour diagrams: $(P-V)\times(X-V)$ (*left*) and $(U-V)\times(Z-V)$ (*right*).

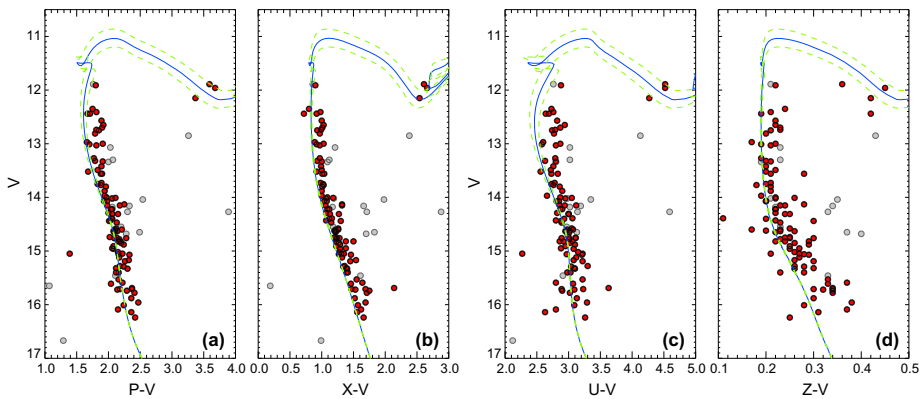

Figure 8. Colour-magnitude diagrams **(a)–(d)** with best fitting PARSEC isochrones. The parameters used are given in Table 4. The solid lines are the best fits, and the dotted lines the one sigma intervals.

stars with parallaxes published in the *Gaia* DR2 and our estimate using the *Gaia* distances for the 99 most probable cluster members together with the relation distance $d = 1000/\varpi$. Gaussian fitting to both these data sets (see Figure 9) led to the estimates given for these studies in Table 4. The estimate from Bailer-Jones *et al.* (2018) is more compatible with the estimate based on the isochrones fitting.

Table 4. Parameters derived in the *Gaia* analysis: 'BJ' stands for the distance (in parsecs) calculated from the *Gaia* DR2 trigonometric parallaxes and stellar distances given by Bailer-Jones *et al.* (2018), 'isochrones' is based on the isochrone fitting described by the paper, and '*Gaia*' on the DR2 distances of the 99 most probable cluster members from this paper. [Fe/H] is the stellar metallicity defined using the total iron content compared to the Solar, while Z is the overall mass fraction for metals (i.e., excluding H and He).

Distance modulus (mag)	Z	[Fe/H] (dex)	Age (Myr)	Isochrones (pc)	*Gaia* (pc)	BJ (pc)
12.85 ± 0.07	0.025	0.24	240 ± 25	2078 ± 78	2460 ± 180	2320 ± 190

4.7 *Mass function*

We obtained a high degree polynomial function between the absolute magnitudes and masses of the main-sequence stars based on the best-fitting PARSEC isochrones. V apparent magnitudes were converted to absolute magnitudes for the main-sequence cluster member stars ($P \geq 0.5$) using the derived distance modulus of the cluster. The member star theoretical masses were calculated from the derived absolute magnitude–mass relation. We obtained the mass function slope from the relation $\log \xi(M) = -(1 + X) \times \log M + C$, where C is a constant. Figure 10 shows the mass function for Melotte 105. The slope of this mass function was obtained from 59 stars whose masses range from 1.90 to 3.52 $M/M_{\odot}$. The mass function slope variable X is -1.42 ± 0.29, which is in very good agreement with $X = -1.35$ value of Salpeter (1955).

4.8 *Galactic orbit*

The galactic orbit of the cluster was calculated using the potential functions that defined in GALPY, the Galactic dynamics library (Bovy 2015).[4] The calculation assumed an axisymmetric potential for the Milky Way galaxy, following MWPOTENTIAL2014 (Bovy 2015). A circular velocity and the galactocentric distance of the Sun were assumed as $V_{\rm rot} = 220$ km/s and $R_{\rm gc} = 8$ kpc (Majewski 1993) respectively.

The MWPOTENTIAL2014 code (Bovy 2015) was used to determine the space velocity components and galactic orbital parameters of the cluster. Calculations require equatorial coordinates, mean distance, proper motion components and radial velocity of Melotte 105. As mentioned in the previous steps in this section, the distance of the cluster is $d = 2078 \pm 78$ pc and the median proper motion values were obtained as $\langle \mu_\alpha \cos\delta \rangle = -6.753 \pm 0.041$ and $\langle \mu_\delta \rangle = 2.156 \pm 0.040$ mas per year. Among the most probable cluster member stars, there are four stars whose radial velocities were available in the literature. The radial velocities of three of the four stars were present in both the Mermilliod *et al.* (2008) (ID 117: $V_R = -4.32 \pm 0.37$ km/s, ID 139: $V_R = 0.54 \pm 0.18$ km/s and ID 184: $V_R = -0.15 \pm 0.31$ km/s) and the *Gaia* DR2 catalogue (ID 117: $V_R = -3.56 \pm 0.84$ km/s, ID 139: $V_R = 9.22 \pm 9.16$ km/s and ID 184: $V_R = 0.63 \pm 1.66$ km/s), while the radial velocity of one star was found only in *Gaia* DR2 (ID 358: $V_R = -0.80 \pm 1.91$ km/s). Where measurements were available in both catalogues, the measurement with the small radial velocity error was preferred by

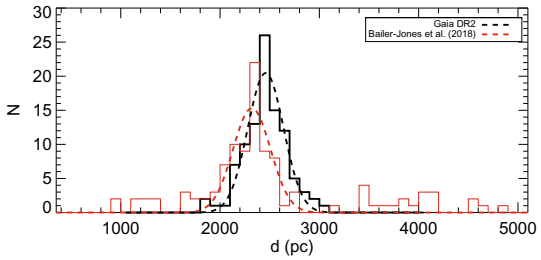

Figure 9. Distance histograms for the Melotte 105 stars with distances calculated by the *Gaia* collaboration and Bailer-Jones *et al.* (2018). The dashed lines are the Gaussian fits to these distance histograms.

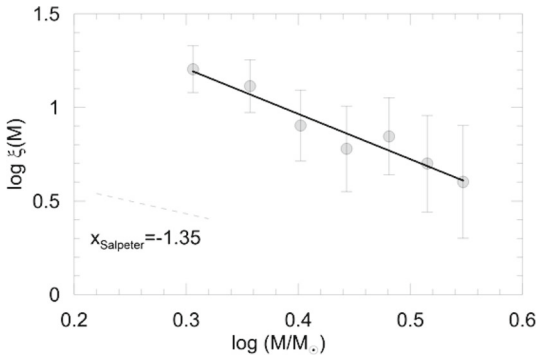

Figure 10. Mass function of Melotte 105 calculated from the most probable main-sequence stars. The solid and dashed lines represent the cluster and Salpeter mass functions respectively.

[4] See also, https://galpy.readthedocs.io/en/v1.5.0/.

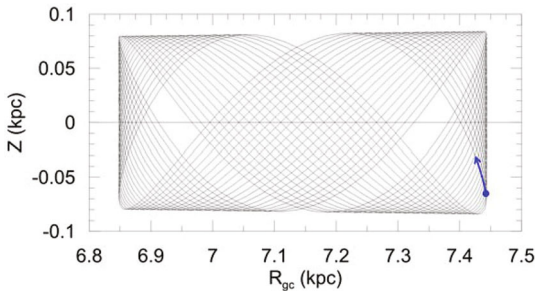

Figure 11. The Galactic orbital motions of Melotte 105 in the $R_{gc} \times Z$ plane. The blue circle and arrow represent the present day position of the cluster and its motion vector, respectively.

this analysis. A weighted average was taken, leading to the cluster mean radial velocity being taken as -1.11 ± 0.14 km/s. Kinematic and dynamic calculations were analyzed with 2 Myr steps over a 3 Gyr integration time.

The space velocity components of the cluster were calculated as $(U, V, W) = (-64.75 \pm 3.34, -26.01 \pm 5.69, -3.12 \pm 0.41)$ km/s. To obtain the space velocity more precisely, the first-order galactic differential rotation correction was taken into account (Mihalas & Binney 1981), with -52.02 and 1.94 km/s differential rotation corrections applied to U and V space velocity components respectively. The W velocity is not affected in this first-order approximation. As for the local standard of rest correction values from Coşkunoğlu *et al.* (2011), $(8.83 \pm 0.24, 14.19 \pm 0.34, 6.57 \pm 0.21)$ km/s were used leading to corrected values of the space velocity components of the cluster of $(U, V, W) = (-3.90 \pm 3.34, -13.76 \pm 5.69, +3.45 \pm 0.41)$ km/s.

Melotte 105's perigalactic and apogalactic distances were obtained as $R_p = 6.85$ and $R_a = 7.44$ kpc, respectively. The maximum vertical distance from the Galactic plane was calculated as $Z_{\max} = 84$ pc and the eccentricity of the orbit was determined as $e = 0.042$.

A representation of the Galactic orbit for Melotte 105 on the $R_{gc} \times Z$ plane is shown in Figure 11. Kinematic and dynamic calculations for the cluster support that the cluster was formed in a metal-rich environment within the Sun circle. Wu *et al.* (2009) gave the cluster distance $d = 2208 \pm 442$ pc and the radial velocity $V_R = 0.4 \pm 0.2$ km/s. These values are similar to those of the current study, but the proper motion components $\langle \mu_\alpha \cos\delta \rangle = -4.37 \pm 0.82$ and $\langle \mu_\delta \rangle = -4.07 \pm 0.96$ mas/yr are different, leading to their orbital parameter estimates being inconsistent with this study. We believe that the use of the *Gaia* DR2 precise astrometric data is an improvement.

5. Conclusions

This paper suggests the need for further study of Melotte 105, although there does appear to be a building convergence towards similar estimates in the literature. Melotte 105 is a suitably populous cluster for a later, careful study investigating completeness and adjusting the mass function suitably to estimate the cluster's initial mass function (similar to Mateo 1987; Sagar and Richtler 1991; Banks *et al.* 1995). In the near future, the Melotte 105 cluster could be studied via high resolution and high S/N spectroscopic observations. The cluster member stars then could be determined using radial velocity analysis, together with the model atmosphere parameters of the member stars and the mean metal abundance being obtained precisely.

The current study is somewhat unusual in that a relatively uncommon photometric system was employed, demonstrating the potential of the Vilnius system to the study of populous clusters. Longer exposure times, a larger telescope, or a combination of both would result in smaller photometric errors in both the cluster and standard star photometry. Together with inclusion of the Y filter, this could lead to a definitive study of the cluster and a final resolution of the discrepancies in the literature.

Acknowledgements

The first author, TB, is grateful for generous time allocations at Mount John University Observatory, the Vilnius Observatory for supplying the filter set, the New Zealand Lottery Board for financing the purchase of the set, the Acorn New Zealand for the loan of a R260 computer on which some of this work was performed and to the Foundation for Research, Science and Technology for partial funding of this project in conjunction with the VUW Internal Research Grant Committee. He also acknowledges partial support during this study by the inaugural R.H.T. Bates Postgraduate Scholarship. The authors would like to thank the anonymous referee for his/her helpful comments and advice which improved this paper. This work has made use of data from the European Space Agency (ESA) mission *Gaia* (https://www.cosmos.esa.int/gaia), processed by the *Gaia* Data Processing and Analysis Consortium (DPAC, https://www.cosmos.esa.int/web/gaia/dpac/consortium). Funding for the DPAC has been provided by national institutions, in particular, the institutions participating in the *Gaia* Multilateral Agreement. IRAF was distributed by the National Optical

Astronomy Observatories, which were operated by the Association of Universities for Research in Astronomy Inc., under contract with the National Science Foundation. It is with sadness the authors note the sudden death of Prof. Denis J. Sullivan (VUW) on Christmas day 2019. Prof. Sullivan was TB's co-supervisor for his Ph.D. and instrumental in starting this project. The authors would like to express their condolences to his family.

References

Ahumada A. V., Claria J. J., Bica E., Piatti A. E. 2000, A&AS, 141, 79
Ak T., Bostancı Z. F., Yontan T. *et al.* 2016, Ap&SS, 361, 126
Bailer-Jones C. A. L., Rybizki J., Fouesneau M., Mantelet G., Andrae E. 2018, AJ, 158, 58
Balaguer-Nunez L., Tian K. P., Zhao J. L. 1998, A&AS, 133, 387
Balona L., Laney C. 1995, MNRAS, 277, 250
Banks T. 1993, Southern Stars, 35, 33
Banks T., Dodd R. J., Sullivan D. J. 1995, MNRAS, 274, 1225
Bilir S., Bostancı Z. F., Yontan T., Güver T., Bakış V., Ak T., Ak S., Paunzen E., Eker Z. 2016, AdSpR, 58, 1900
Bostancı Z. F., Yontan T., Bilir S., Ak T., Güver T., Ak S., Paunzen E., Başaran Ç. S., Vurgun E., Akti B. A., Çelebi M., Ürgüp H. 2018, Ap&SS, 363, 143
Bovy J. 2015, ApJS, 216, 29
Boyle R. P., Smriglio F., Nandy K., Straižys V. 1990a, A&AS, 84, 1
Boyle R. P., Smriglio F., Nandy K., Straižys V. 1990b, A&AS, 86, 395
Boyle R. P., Dasgupta A. K., Smriglio F., Straižys V., Nandy K. 1992, A&AS, 95, 1
Boyle R. P., Vrba F. J., Smriglio F., Dasgupta A. K., Straižys V., 1996, Baltic Astron., 5, 231
Bressan A., Marigo P., Girardi L., Salasnich B., Dal Cero C., Rubele S., Nanni A. 2012, MNRAS, 427, 127
Černies K., Meištas E., Straižys V., Zdanavičus V. 1989, Bull. Vilnius Obs., 84, 1
Černies K., Zdanavičus V., 1992, Baltic Astron., 1, 83
Chen Y., Girardi L., Bressan A., Marigo P., Barbieri M., Kong X. 2014, MNRAS, 444, 2525
Coşkunoğlu B., Ak S., Bilir S. *et al.* 2011, MNRAS, 412, 1237
Dias W. S., Monteiro H., Caetano T. C., Oliveira A. F. 2012, A&A, 539, A125
Dodd R. J., Forbes M. C., Sullivan D. J. 1993, in Stellar Photometry – Current Techniques and Future Developments, IAU Colloquium #136, eds, C. J. Butler & I. Elliot, Cambridge University Press, Cambridge, 51
Forbes M. C. 1993, Southern Stars, 35, 69
Forbes M. C. 1996, Unpublished, Ph.D. thesis, Victoria University of Wellington, New Zealand
Frandsen S., Dreyer P., Kjeldsen H. 1989, A&A, 215, 287
Harris W. E., FitzGerald M. P., Reed B. C. 1981, PASP, 93, 507
Javakhishvili G., Kukhianidze V., Todua M., Inasaridze R. 2006, A&A, 447, 915
King I. 1962, AJ, 67, 471
Kjeldsen II., Frandsen S. 1991, A&AS, 87, 119
Krone-Martins A., Moitinho A. 2014, A&A, 561A, 57
Majewski S. R. 1993, ARA&A, 31, 575
Mateo M. 1987, ApJ, 323, L41
Mermilliod J. C., Mayor M., Udry S. 2008, A&A, 485, 303
Mihalas D., Binney J. 1981, Galactic Astronomy: Structure and Kinematics, San Francisco: Freeman, 2nd edition
Monteiro H., Dias W. S., Caetano T. C. 2010, A&A, 516, A2
Moore C. H. 1974, A&AS, 15, 497
Munari U., Fiorucci M. 2003, Mem. S.A.It, 74, 151
Oliveira A. F., Monteiro H., Dias W. S., Caetano T. C. 2013, A&A, 557, A14
Paunzen E., Netopil M. 2006, MNRAS, 371, 1641
Piatti A. E., Claria J. J. 2001, A&A, 370, 931
Sagar R., Munari U., de Boer K. S. 2001, MNRAS, 327, 23
Sagar R., Richtler T. 1991, A&A, 250, 324
Santos J. F. C. Jr., Bica E. 1993, MNRAS, 260, 915
Salpeter E. E. 1955, ApJ, 121, 161
Sher D. 1965, MNRAS, 129, 17
Straižys V., Sviderskienė, Z. 1972, Bull. Vilnius. Astron. Obs., 35, 1
Straižys V. 1974, A&A, 36, 435
Straižys V. 1992a, Multicolor Stellar Photometry, vol. 15, Astronomy & Astrophysics Series, Pachart, Tucson
Straiž y V. 1992b, Baltic Astron., 1, 107
Stetson P. B. 1987, PASP, 99, 191
Tang J., Bressan A., Rosenfield P., Slemer A., Marigo P., Girardi L., Bianchi L. 2014, MNRAS, 445, 4287
Tobin W. 1992, Southern Stars, 34, 421
Wells D. C., Greisen E. W., Harten R. H. 1981, A&AS, 44, 363
Wu Z.-Yu, Zhou X., Ma J., Du C.-H. 2009, MNRAS, 399, 2146
Yadav R. K. S., Sagar R. 2002, MNRAS, 337, 133
Yontan T., Bilir S., Bostancı Z. F., Ak T., Ak S., Güver T., Paunzen E., Ürgüp H., Çelebi M., Akti B. A., Gökmen S. 2019, Ap&SS, 364, 152
Zdanavičus V., Sudžius J., Sviderskienė Z., Straižys V., Burnašov V., Drazdys R., Bartkevičius A., Kakaras G., Kavalianskaite G., Jasevičius V. 1969, Bull. Vilnius Obs., 26, 3